Organic & Biomolecular Chemistry

Cite this: *Org. Biomol. Chem.*, 2011, **9**, 2760

www.rsc.org/obc

PAPER

A DFT study on the mechanism of gold(III)-catalyzed synthesis of highly substituted furans *via* [3, 3]-sigmatropic rearrangements and/or [1, 2]-acyloxy migration based on propargyl ketones†

Ran Fang,*[a] Lizi Yang[a] and Yongcheng Wang[b]

Received 30th November 2010, Accepted 25th January 2011
DOI: 10.1039/c0ob01098g

The mechanisms of gold(III)-catalyzed synthesis of highly substituted furans *via* [3,3]-sigmatropic rearrangements and/or [1,2]-acyloxy migration based on propargyl ketones have been investigated using density functional theory calculations at BHandHLYP/6-31G(d,p) (SDD for Au) level of theory. Solvent effects on these reactions were explored using calculations that included a polarizable continuum model (PCM) for the solvent (toluene). Two plausible pathways that lead to the formation of Au(III) vinyl carbenoid and an allenyl structure through [3,3]-sigmatropic rearrangements, [1,2]-acyloxy migration *via* oxirenium and dioxolenylium were performed. Our calculated results suggested: (1) the major pathway of the cycle causes an initial Rautenstrauch-type [1,2]-migration *via* oxirenium to form an Au(III) vinyl carbenoid. Subsequent cycloisomerization of this intermediate then provides the corresponding furan whether for the methyl-substituted propargylic acetates or the phenyl-substituted propargylic acetates; (2) for the methyl-substituted propargylic acetates, the formation of Au(III) vinyl carbenoid structures was the rate-determining step. However, intramolecular nucleophilic attack and subsequent cycloisomerization to give the final product was rate-determining for the phenyl-substituted propargylic acetates. The computational results are consistent with the experimental observations of Gevorgyan, *et al.* for gold(III)-catalyzed synthesis of highly substituted furans based on propargyl ketones.

1. Introduction

Highly substituted furans are an important group of heteroaromatic compounds found in many natural products and substances that have useful industrial applications.[1] They are also often used as synthetic intermediates in the preparation of acyclic, carbocyclic, and heterocyclic compounds.[2] Therefore, there has been much effort aimed at the development of efficient synthetic methodologies for their preparation.[3–9] As we know, alkynes are the most versatile substrates that are easily accessible to propargylic esters.[10–11] Notably, their propensity to undergo [1,2]- and [3,3]-acyloxy migration, which thereafter leads to the formation of an Au(III) vinyl carbenoid and to an allenyl structure, respectively, both poised for subsequent functionalization, allows for great structural diversity. It is widely accepted that terminal or electron-poor alkynes react *via* a [1,2]-migration pathway,[12–13] whereas internal alkynes prefer the [3,3]-migration pathway.[14] So far only a few exceptions to this general pattern have been described.[15–16]

On the other hand, gold homogeneous catalysis has not only been the subject of numerous theoretical studies but has also been practically applied to organic chemistry.[17] Recently, Gevorgyan *et al.* studied gold(III)-catalyzed isomerization of propargylic acetates by ^{17}O labelling experiments in the context of cycloisomerization of ynones to furans under mild conditions[18] According to the experimental results, two general mechanisms were postulated to explain the formation of furans from propargyl-substituted ketones. As depicted in the Scheme 1, **A** first undergoes a [3,3]- shift to form allenyl structure **B**. The first mechanism operates *via* an allenyl intermediate **B** whereas the second goes through carbenoid species **D** (Scheme 1). A subsequent 1,2-shift *via* a dioxolenylium species would reach furan **C**. Alternatively, if **A** undergoes a [1,2]-shift to form metal carbenoid **D**, the intermolecular nucleophilic attack and subsequent cycloisomerization of this intermediate then provides the corresponding furan product **E**.

To the best of our knowledge, there are no detailed theoretical studies available in the literature for the novel gold(III)-catalyzed transformation reported by Gevorgyan *et al.* [18] Hence, we present a thorough density functional theory (DFT) computational investigation of the mechanism of the gold(III)-catalyzed synthesis of highly substituted furans based on the experimental evidence reported by Gevorgyan *et al.* [18] The present DFT study located the transition states for the reactions of interest and performed

[a]*College of Chemistry and Chemical Engineering, Lanzhou University, Lanzhou, 730000, P. R. China. E-mail: fangr@lzu.edu.cn*
[b]*College of Chemistry and Chemical Engineering, Northwest Normal University, Lanzhou, 730070, P. R. China*

† Electronic supplementary information (ESI) available: Supporting information. See DOI: 10.1039/c0ob01098g

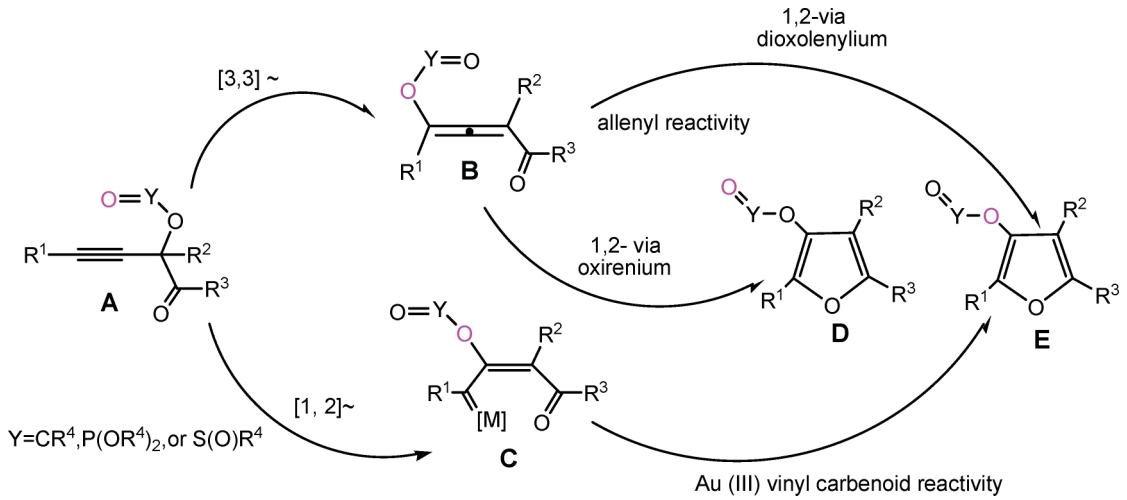

Scheme 1 Two plausible mechanisms were envisioned for this novel gold(III)-catalyzed transformation.

a vibrational analysis at these stationary points. From the results shown here, we expect to learn more about the factors that control the activation barriers of this important reaction, and further investigate the effects of solvent on the thermodynamic and kinetic properties of these reactions.

2. Results and discussion

Energy profiles for reaction pathways **a**, **b** and **c** are shown in Fig. 1, 2 and 3. The optimized geometries for the reactants (R1: $AuCl_3$; R2: propargyl ketone), intermediates, transition states and products of the reactions are depicted schematically in Fig. 4 along with selected key geometry parameters (*e.g.* bond lengths). Their relative energies and free energies in the gas and solution phases, together with the activation barriers corresponding to the relevant transition structures, are shown in Table 1. Unless otherwise noted, the relative energies discussed in subsequent sections refer to the value in toluene solvent. The detailed structural parameters and energies for the structures determined here are collected in the Supporting information.†

2.1 Pathway a: [3,3]-sigmatropic rearrangements

The energy profile for this process is represented in Fig. 1. The structures of the various critical points located on the potential surface along with the values of the most relevant geometry parameters are shown in Fig. 4. From the energy profile it is evident that the first step of pathway **a** involves a preliminary intermediate **1** where the terminal carbon–carbon triple bond of the substrate interacts with the gold atom. If we consider $AuCl_3$ as the "active" structure of the catalyst, **1** forms without any barrier and is 15.0 kcal mol^{-1} lower in energy than the reactants [$AuCl_3$ (R1) + propargyl ketone (R2)]. In **1**, this is a polarized complex with distances between Au and two sp-hybridized carbon atoms of 2.389 and 2.298 Å, respectively. Furthermore, the C^1–C^2 bond has lost a little of its triple bond character and is now 1.219 Å (1.201 Å in R2). Once in **1**, the coordination of the triple bond with the gold atom induces a cyclization of the carbonyl oxygen (O^2) onto the triple bond (C^1). A new and stable oxonium ion structure **2a** is formed through a six-membered ring transition structure **TSa1** (**TSa1** has only one imaginary frequency of 148 i cm^{-1} and IRC calculations confirmed that this TS connects the corresponding reactants and intermediate). Such six-membered ring transition structures were also found in the reactions of Au(I)-catalyzed skeletal rearrangement and cycloadditions of enynes and cyclopropyl propargylic carboxylates.[13,19] Inspection of Fig. 1 shows that the gold atom is completely connected with the C^2 atom of the propargyl ketone (the bond distance Au–C^2 is 2.122 Å) in **TSa1** and the bond of the C^1–C^2 changes from 1.219 to 1.250 Å. In **TSa1**, nucleophilic attack of O^2 on the positively charged C^1 leads to the formation of C^1–O^2 bond and the distance of C^1–O^2 in **TSa1** was 2.217 Å. Moreover, the transition vector obtained from the frequency computations on **TSa1** is dominated by the C^1–O^2 and C^1–C^2 distances. Table 1 showed that the free energy of activation was calculated to be 1.5 kcal mol^{-1} for **TSa1** and the free energy of reaction was −19.5 kcal mol^{-1} for the **2a** with respect to **1**. In **2a**, it is evident that the C^3–O^1 and the C^1–O^2 bonds are weaker than that of a normal C–O single bond (1.43 Å), as demonstrated by their long bond lengths of 1.478 and 1.445 Å, respectively. The fact that the C^3–O^1 bond is breaking and the C^1–O^2 bond is forming may account for the phenomenon. The C^1–C^2 triple bond completes its change from a triple bond to a double bond (1.317 Å). Due to the ring strain of six-membered ring, the oxonium ion structure **2a** is then converted to the allenyl structure **3a** *via* a four-electron rearrangement transition structure **TSa2**. In **TSa2**, the breaking C^3–O^1 bond is 2.312 Å. The activation free energy of the second step was 20.0 kcal mol^{-1}, and the formation of **3a** is an endothermic process (the free energy of reaction for the **3a** was 9.9 kcal mol^{-1} with respect to **2a**). Intermediate **3a** can also be regarded as a π-complex between Au(III) and carboxyallene and such a structure was also found in the reactions of Au(I)-catalyzed skeletal rearrangement and cycloadditions of enynes.[5,11] To accomplish a cyclization of the carbonyl oxygen onto the double bond, subsequent coordination of the carbonyl oxygen with $AuCl_3$ resulted in formation of new intermediates **4a** where the carbonyl oxygen interacts with the gold atom. **4a** was 0.7 kcal mol^{-1} lower in energy than **3a** and remained 10.3 kcal mol^{-1} lower than the reactants. This indicates that the carbonyl oxygen atom

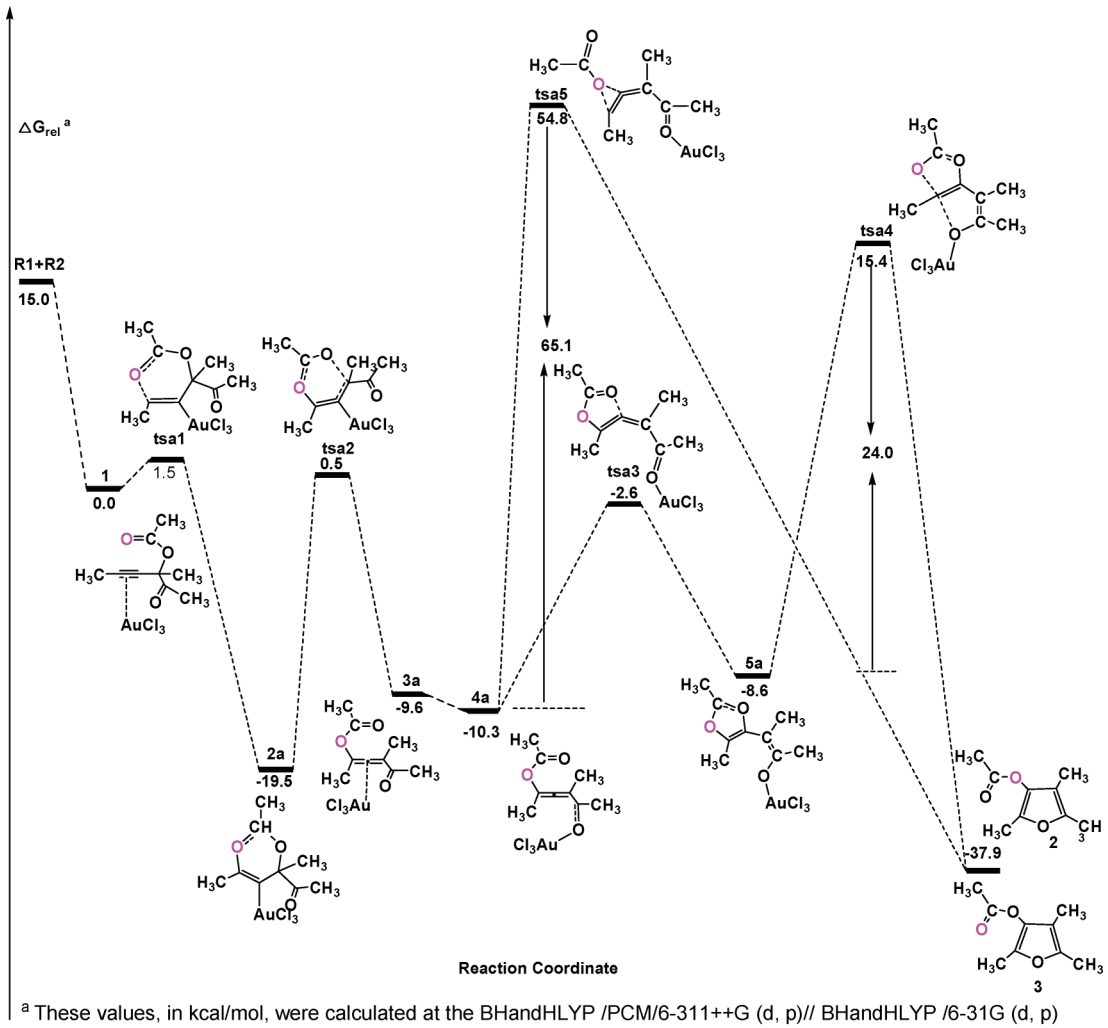

Fig. 1 Energy profiles for path a; the relative energies are given in kcal mol^{-1}.

interaction with the gold atom is significantly stronger than that between the gold atom and the C≡C triple bond. Examination of Fig. 4 shows that the bond of Au–O^3 was 2.080 Å and the interaction of Au atom with the carbonyl oxygen makes the C^4–O^3 bond elongated to 1.236 Å in **4a**. Subsequently, [1,2]-migration *via* oxirenium structures would provide the product furan **2**, whereas [1,2]-migration *via* dioxolenylium structures produces furan **3**.

In **4a**, the nucleophilic attack of O^1 on the positively charged C^2 leads to the formation of the five-membered ring of oxonium ion structure **5a** through **TSa3**. The activation free energy of this step was 7.7 kcal mol^{-1} and the formation of **5a** was also an endothermic process (the free energy of reaction for the **5a** was 1.7 kcal mol^{-1} with respect to **4a**). There is subsequent nucleophilic attack of O^3 on the positively charged C^1 to accomplish a cyclization of the carbonyl oxygen onto the double bond, leading to the formation of the final product **3** and regeneration of the catalyst (R1) through **TSa4**. Table 1 shows that the free energy of activation for this step was calculated to be 24.0 kcal mol^{-1} for **TSa4** and these final steps were exothermic by –29.3 kcal mol^{-1}. In total, the whole catalytic process was exothermic by –52.9 kcal mol^{-1}, lower than reactants ($AuCl_3$ (R1) + propargyl ketone (R2)). Note that this step is rate-determining.

The route of **TSa3** for [1,2]-migration occurs *via* oxirenium structures, but concerted [1,2]-migration *via* dioxolenylium structures process is also a possible pathway. Inspection of Table 1 shows that the free energy of activation for this step is calculated to be 65.1 kcal mol^{-1} for **TSa5**, that these final steps are exothermic by –27.6 kcal mol^{-1} and the whole catalytic process was exothermic by –52.9 kcal mol^{-1}, lower than reactants ($AuCl_3$ (R1) + propargyl ketone (R2)). The higher barrier found for **TSa5** indicates that this step is rate-determining for the whole catalytic process, rendering the pathway for **TSa4** more feasible than that of **TSa5**.

2.2 Pathway b:[1,2]-acyloxy migration *via* oxirenium

Apart from [3,3] -sigmatropic rearrangements, Rautenstrauch-type [1,2]-migration *via* oxirenium gives rise to another possible reaction pathway. The energy profile for this process is depicted in Fig. 2. The structures of the various critical points located on the potential surface along with the values of the most

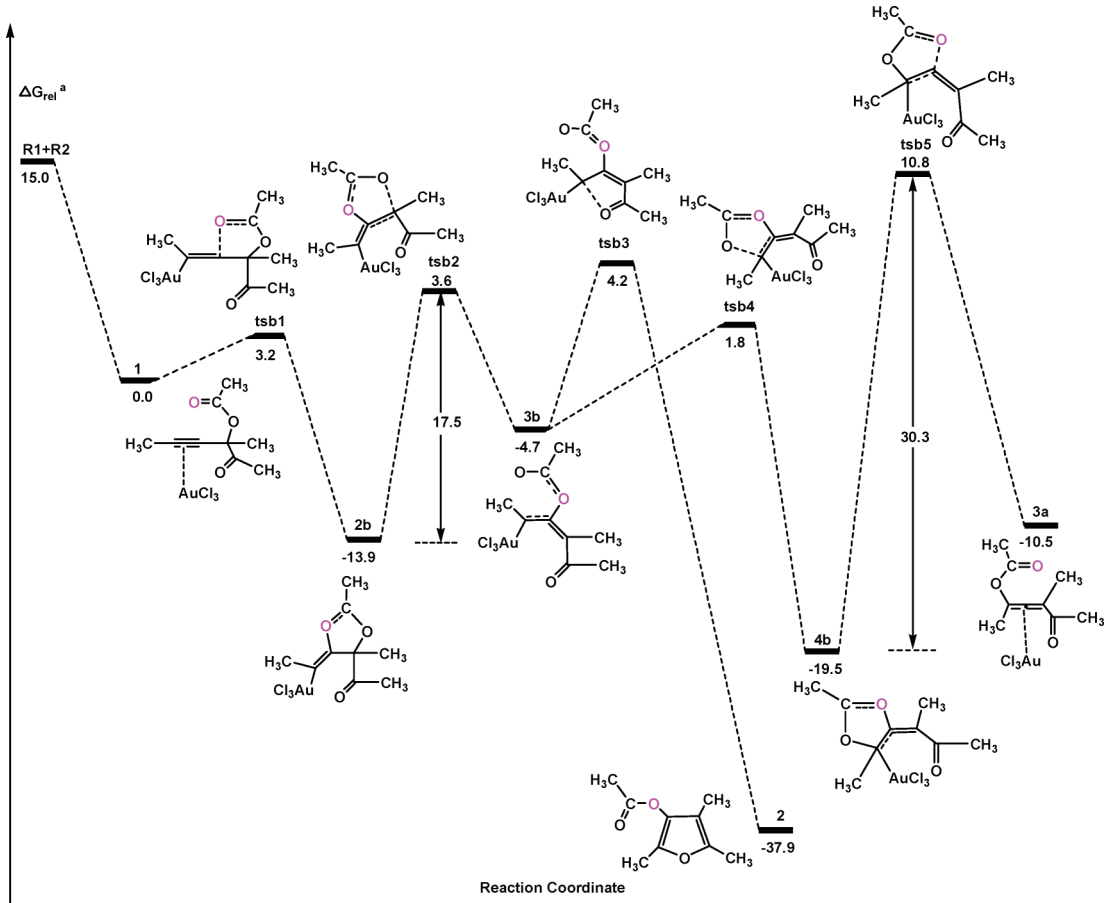

[a] These values, in kcal/mol, were calculated at the BHandHLYP /PCM/6-311++G (d, p)// BHandHLYP /6-31G (d, p) (SDD for Au) level of theory using single-point PCM calculations to model the effect of the solvent (toluene)

Fig. 2 Energy profiles for path **b**; the relative energies are given in kcal mol^{-1}.

relevant geometry parameters are presented in Fig. 4. Examination of Fig. 2 shows that the first step for pathway **b** involves a preliminary intermediate **1**. Cyclization of the carbonyl oxygen (O^2) onto the triple bond (C^2) gives a new and stable oxonium ion structure **2b** through a five-membered ring transition structure **TSb1**. Such five-membered ring transition structures were also found in the reactions of Au(I)-catalyzed skeletal rearrangement and cycloadditions of enynes.[13] Inspection of Fig. 2 shows that the gold atom is completely connected with the C^1 atom of the propargyl ketone (the bond distance Au–C^1 is 2.138 Å) in **TSb1** and the bond of the C^1–C^2 changes from 1.219 to 1.247 Å. In **TSb1**, nucleophilic attack of O^2 on the C^2 leads to the formation of the C^2–O^2 bond and the distance of C^2–O^2 in **TSb1** is 2.187 Å. In Table 1 the free energy of activation for this step is calculated to be 3.2 kcal mol^{-1} for **TSb1** and the free energy of reaction for the **2b** intermediates is −13.9 kcal mol^{-1} with respect to **1**. The higher barriers found for **TSb1** compared to those of **TSa1** can be mainly attributed as follows. The NBO charges on the C^1, C^2 and O^2 atoms are 0.26, −0.07 and −0.48 au, respectively. A positive charge found for the C^1 atom makes nucleophilic attack of O^2 on the positively charged C^1 more feasible than on the C^2 atom. As exhibited by the structure of **2a**, the C^3–O^1 and the C^2–O^2 bonds in **2b** are also weaker than a normal C–O single bond (1.43 Å); now are 1.478 and 1.445 Å, respectively. Furthermore, the C^1–C^2 bond also accomplishes a conversion of triple bond to double bond; now the bond distance is 1.313 Å. The subsequent step for cleavage of the C^3–O^1 bond generates the Au(III) vinyl carbenoid structures **3b** through **TSb2**. Similar intermediates have also been observed to be trapped by other electrophiles in an intramolecular fashion.[20–22] The activation free energy of the second step is 17.4 kcal mol^{-1}, and the formation of **3b** is an endothermic process (the free energy of reaction for the **3b** was 9.2 kcal mol^{-1} with respect to **2b**), which indicates that this step is rate-determining. Fig. 4 shows that the C^3–O^1 bond changes from 1.500 to 2.136 Å in **TSb2**. Furthermore, the C^2–C^3 bond has lost its single bond character and is now 1.426 Å. As the reaction goes from **TSb2** to **3b**, the C^3–O^1 bond is completely broken in **3b**. The Au(III) vinyl carbenoid structure **3b**, undergoes intramolecular nucleophilic attack and subsequent cycloisomerization to give the final product **2** and regeneration of the catalyst (R1) (**TSb3**) but also undergoes a subsequent [1,2]-migation to give the allenyl structure **3a** (**TSb4**). Table 1 shows that the free energy of activation for intramolecular nucleophilic attack (**TSb3**) is calculated to be 8.9 kcal mol^{-1} and the formation of final product **2** is an exothermic process (the free energy of reaction for **2** is −33.2 kcal mol^{-1} with respect to **3b**). The whole catalytic process was exothermic by −52.9 kcal mol^{-1}, lower than reactants. As is shown in Fig. 4, **TSb3** has a similar structure to **3b**. For instance, the C^1–C^2 and C^4–O^3 bond are only elongated by

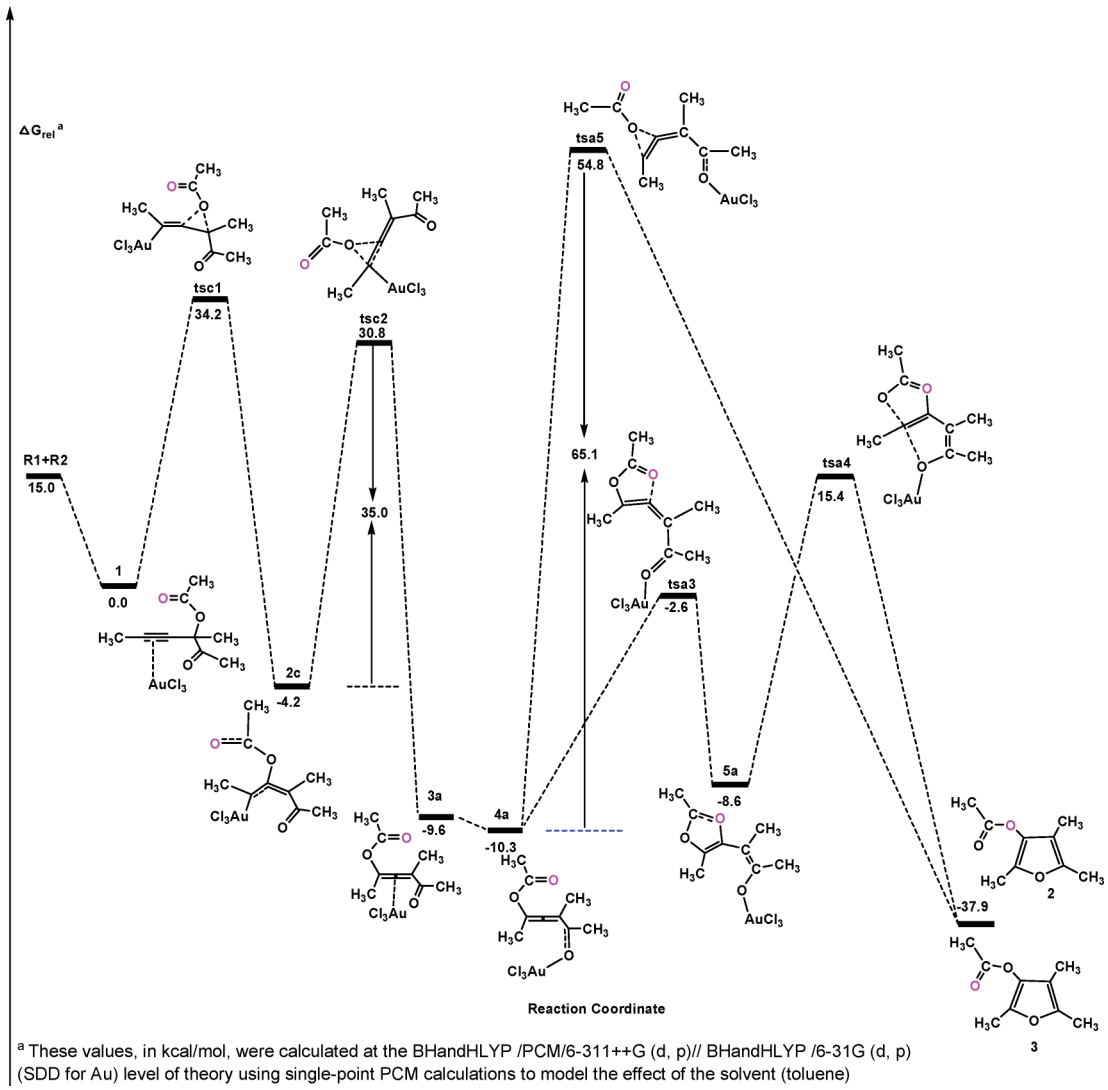

Fig. 3 Energy profiles for path **c**; the relative energies are given in kcal mol^{-1}.

0.05 and 0.003 Å, respectively. These structural features reveal that transition structures of **TSb3** take on more reactant-like character than product-like character. According to Hammond[23] this step should have lower activation barriers, which is consistent with our calculated results.

The Au(III) vinyl carbenoid structure **3b** can also undergo a subsequent [1,2]-migation to give the allenyl structure **3a**. Nucleophilic attack between O^1 and C^1 leads to a new oxonium ion structure **4b** through five-membered ring transition structures **TSb4**. In **TSb4**, the distance of C^1–O^1 bond was 2.275 Å and the C^1–C^2 bond was also elongated to 1.441 Å. From Table 1 we can see that the free energy of activation for this step is calculated to be 6.5 kcal mol^{-1} for **TSb3** and the reaction free energy is –14.8 kcal mol^{-1} with respect to **3b**. The next step for breaking the C^2–O^2 bond gives the allenyl structure **3a** through compound **TSb5**. The activation free energy of this step was 30.3 kcal mol^{-1} and the formation of **3a** was an endothermic process (the free energy of reaction for **3a** was 9.0 kcal mol^{-1} with respect to **4b**). It is therefore obvious that this step is rate-determining for this pathway. The higher barriers found for **TSb5** indicate that the formation of allenyl structure **3a** through **TSb5** is unfavorable.

2.3 Pathway c: [1,2]-acyloxy migration *via* dioxolenylium

It has been suggested that double [1,2]-acyloxy migrations *via* dioxolenylium can also account for the formation of **3a**. In order to investigate this assertion, pathway **c**: [1,2]-acyloxy migration *via* dioxolenylium was performed. The energy profile for this process is represented in Fig. 1. The structures of the various critical points located on the potential surface along with the values of the most relevant geometry parameters are shown in Fig. 4. Examination of Fig. 3 suggests that a first step for pathway **c** also involves a preliminary intermediate **1**. Then, double [1,2]-migrations *via* dioxolenylium structures and Au(III) vinyl carbenoid structures **2c** gives the allenyl structure **3a** through **TSc1** and **TSc2**. The activation free energy of the first [1,2]-migration *via* dioxolenylium structure step was 34.2 kcal mol^{-1} and the reaction free energy was –9.6 kcal mol^{-1} with respect to **1**. In **TSc1**, the

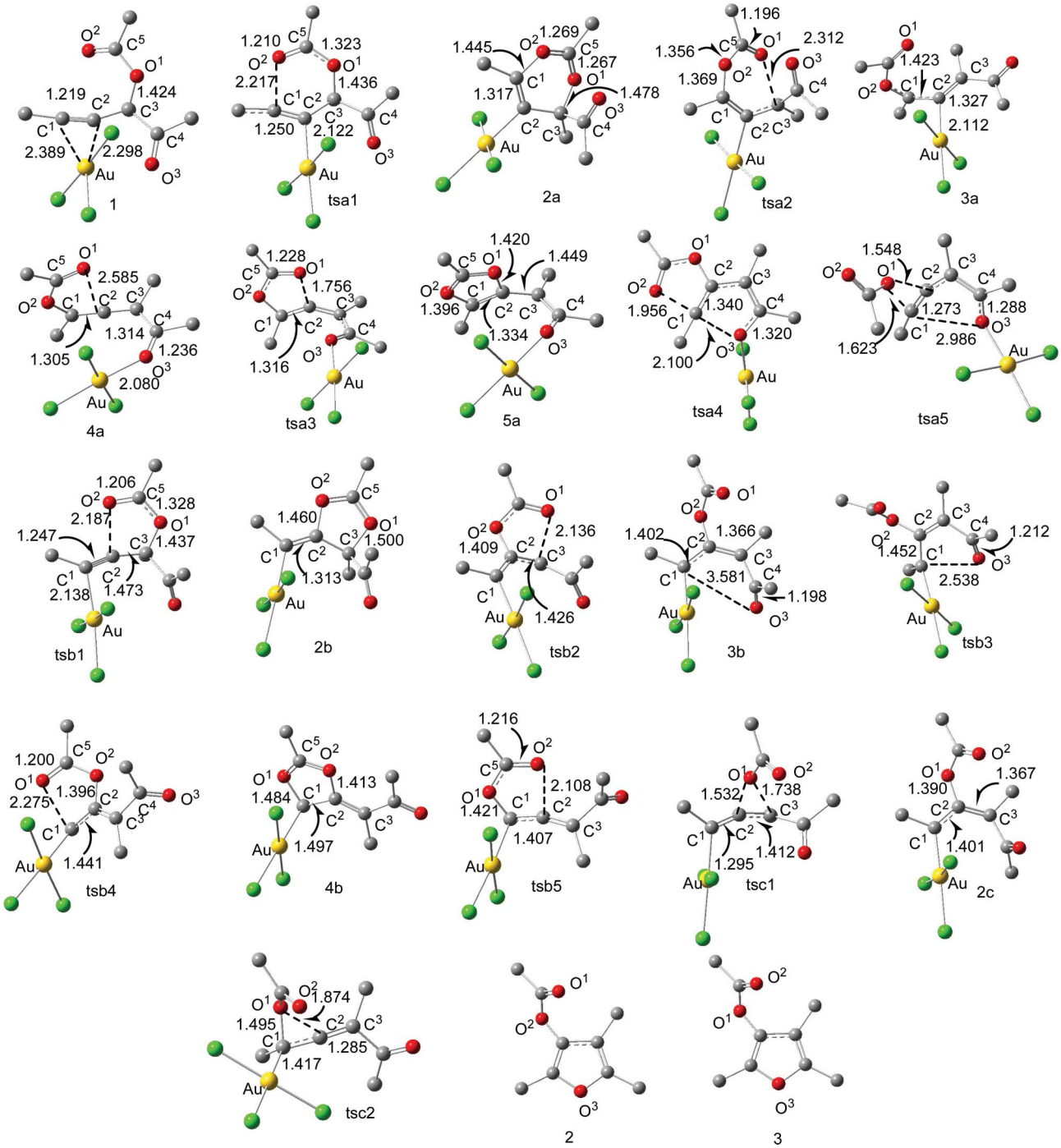

Fig. 4 Optimized structures for path **a**, **b** and **c** shown in Fig. 1, 2 and 3 with selected structural parameters (hydrogen atoms are omitted for clarity and bond lengths are presented in Å).

distances of C^2–O^1 and C^3–O^1 were 1.532 and 1.738 Å, respectively. After the formation of **2c**, subsequent pathways for [1,2]-acyloxy migration *via* oxirenium or intramolecular nucleophilic attack and subsequent cycloisomerization to give the final product **3** are already discussed in the above paragraphs. In this section, only the second [1,2]-migration *via* dioxolenylium structure step (**TSc2**) for formation of allenyl structure **3a** is discussed. Inspection of Fig. 4 shows that **TSc2** has a similar structure to the **TSc1** long C–O bond, (C^2–O^1 and C^1–O^1 bonds were 1.874 and 1.495 Å, respectively). The activation free energy of this step was 35.0 kcal mol^{-1} and the formation of **3a** was an endothermic process (the free energy of reaction for the **3a** was 5.4 kcal mol^{-1} with respect to **2c**). This step is rate-determining for this reaction pathway.

Table 1 Thermodynamic properties (Relative Free Energy and Activation Free Energy in gas phase and in solution) of the structures in Fig. 1, 2 and 3[a]

System	ΔE^{rel}_{gas}	$\Delta E^{\neq}_{gas}$	ΔG^{rel}_{gas}	$\Delta G^{\neq}_{gas}$	ΔE^{rel}_{sol}	$\Delta E^{\neq}_{sol}$	ΔG^{rel}_{sol}	$\Delta G^{\neq}_{sol}$
1	0.0	0.0	0.0	0.0	0.0	0.0	0.0	0.0
TSa1	2.3	2.3	3.1	3.1	2.7	2.7	1.5	1.5
2a	−18.0		−15.4		−19.5		−19.5	
TSa2	1.7	2.0	19.7	17.4	2.4	0.5	0.5	20.0
3a	−8.6		−7.9		−9.0		−9.6	
4a	−11.6		−11.3		−11.6		−10.3	
TSa3	0.7	12.3	0.1	11.4	2.1	12.5	−2.6	7.7
5a	−7.6		−6.3		−5.3		−8.6	
TSa4	17.4	25.0	18.2	24.6	19.7	25.5	15.4	24.0
TSa5	56.3	67.9	55.7	67.0	58.9	69.3	54.8	65.1
TSb1	3.5	3.5	4.2	4.2	3.8	3.8	3.2	3.2
2b	−8.7		−7.7		−11.9		−13.9	
TSb2	4.8	13.5	6.6	14.2	4.5	16.4	3.6	17.4
3b	−2.6		−2.9		−2.8		−4.7	
TSb3	5.6	8.2	6.9	9.8	6.2	9.0	4.2	8.9
TSb4	3.0	5.6	3.9	6.8	2.6	5.4	1.8	6.5
4b	−16.5		−14.7		−18.6		−19.5	
TSb5	11.2	27.6	12.1	26.8	11.0	29.7	10.8	30.2
TSc1	38.9	38.9	38.9	38.9	38.0	38.0	34.2	34.2
2c	−1.9		−2.4		−2.1		−4.2	
TSc2	32.3	34.2	33.1	35.5	32.9	35.0	30.8	35.0
3a	−8.6		−7.9		−9.0		−9.6	
2	−38.5		−35.9		−37.9		−37.9	
3	−38.5		−35.9		−37.9		−37.9	

[a] These values, in kcal mol^{-1}, were calculated at the BHandHLYP/6-31G(d,p) (SDD for Au) level of theory and included the zero-point energy correction, using single-point PCM calculations at the BHandHLYP/PCM/6-311++G(d,p)//BHandHLYP/6-31G(d,p) (SDD for Au) level of theory to model the effect of the solvent.

2.4 General reactivity: allenyl structures *vs.* Au(III) vinyl carbenoid structures

It is known that under Au catalysis, gold propargylic esters structures such as **A** undergo [1,2]- and [3,3]-acyloxy migration,[12–16] leading to the formation of allenyl structures as **B** and gold vinyl carbenoid structures as **D** (Scheme 1). Of course, the formation of allenyl structures **B** and gold vinyl carbenoid structures **D** have also been proposed as key steps in the Au-catalyzed propargylic esters structures. For the title reaction, all three plausible pathways involved [3,3]-sigmatropic rearrangements. [1,2]-acyloxy migration *via* oxirenium and dioxolenylium leading to an allenyl structure. However, only pathway **b** that involved [1,2]-acyloxy migration *via* oxirenium is responsible for the formation of the gold vinyl carbenoid structure. Inspection of Table 1 shows that the activation free energy for the formation of allenyl structures (**TSa2**, **TSb5** and **TSc2**) were 20.0, 30.3 and 35.0 kcal mol^{-1}, respectively. The activation free energy for the formation of gold vinyl carbenoid structures (**TSb2**) is only 17.4 kcal mol^{-1}. The lower barriers found for **TSb2** indicate that the gold vinyl carbenoid structure plays an important role in the whole reaction.

2.5 [3,3]-sigmatropic rearrangements or [1,2]-acyloxy migration?

According to experimental results, two general mechanisms have been postulated to explain the formation of furans from propargyl-substituted ketones. The first operates *via* an allenyl structure **2** whereas the second goes *via* the carbenoid structure **D** (Scheme 1). If one oxygen in the migrating group is selectively labeled, as shown in **A**, it is possible to distinguish between the two mechanistic pathways. Thus, as depicted in the upper pathway, **A** first undergoes a [3,3]-shift, with "inversion" of the labeled oxygen to form allenyl structure **B**. A subsequent 1,2-shift *via* a dioxolenylium species will result in a second "inversion" to produce the Y=O oxygen-labeled furan **C**. Alternatively, if **1** undergoes a [1,2]-shift to form a metal carbenoid **D**, the label will be located at the bridged oxygen atom. Intermolecular nucleophilic attack and subsequent cycloisomerization proceeds with no migration, so the label will remain at the bridged oxygen position in the furan product **E**. Thus, labelled acetate **A** was tested under several reaction conditions, so proving efficiency in catalyzing this transformation. More remarkably, the reactions using $AuCl_3$ gave **E** exclusively. Based on the results of the labelling studies, transition metal catalysts such as Au(III) are likely to cause an initial [1,2]-migration through a five-membered ring transition state to form a metal carbenoid (Scheme 1, lower pathway). Subsequent cycloisomerization of this intermediate provides the corresponding furan. As is known, the actual pathway followed to reach **2** and **3** is determined by the energy difference between the transition states of highest energy along the different pathways. According to our calculated results, **TSa4** and **TSb2** play vital roles in the title reaction. Moreover, the relative energy difference between the activation energies of **TSb2** and **TSa4** is 6.6 kcal mol^{-1}, which suggests that the first step of the cycle will cause an initial Rautenstrauch-type [1,2]-migration *via* a five-membered ring transition state to form an Au(III) vinyl carbenoid. Subsequent cycloisomerization of this intermediate then provides the corresponding furan **2**. Our calculated results are in good agreement with the experimental observations of Gevorgyan *et al.* [18]

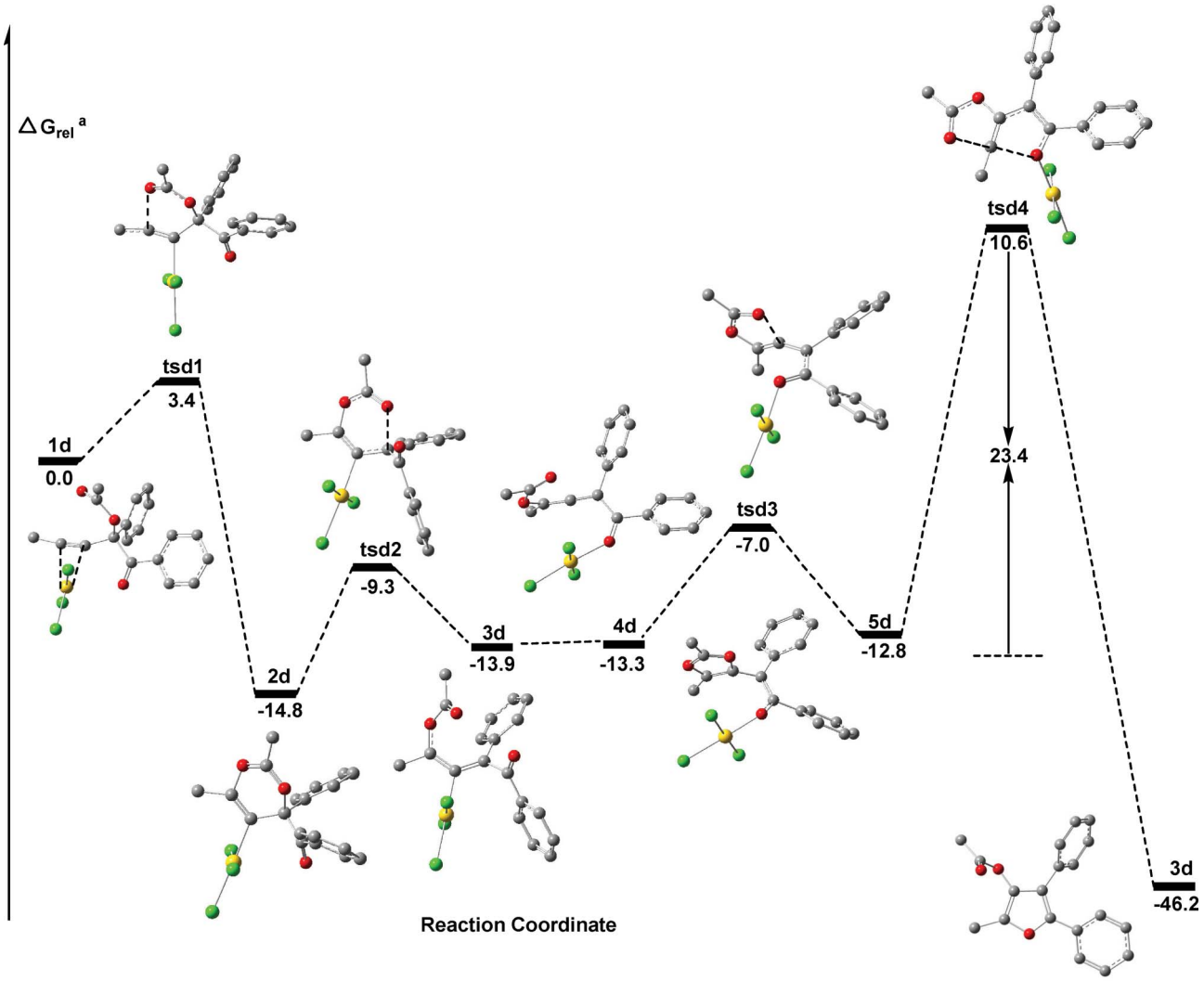

[a] These values, in kcal/mol, were calculated at the BHandHLYP /PCM/6-311++G (d, p)// BHandHLYP /6-31G (d, p) (SDD for Au) level of theory using single-point PCM calculations to model the effect of the solvent (toluene)

Fig. 5 Energy profiles for path **a** of the phenyl-substituted propargylic acetates; the relative energies are given in kcal mol^{-1} (hydrogen atoms are omitted for clarity).

2.6 Effect of the substitution

In the original experimental paperref. 18, the authors employed phenyl-substituted propargylic acetates as the substrates and this different substitution may have an important effect on the reaction mechanism. In order to further account for the effect of the substitution, the reaction pathways **a** and **b** for the phenyl-substituted propargylic acetates were calculated and the energy profile for this process is represented in Fig. 5 and 6. Examination of Fig. 5 shows that a lower barrier is found for **TSd2** (20.0 and 4.5 kcal mol^{-1} for the methyl-substituted propargylic acetates and the phenyl-substituted propargylic acetates, respectively) going from the intermediates to the transition states than for **TSa2**. The lower barriers found for **TSd2** may be due to the following: First, the DFT calculations show that the breaking of the C–O bond in **TSd2** and **TSa2** structures stretched this bond distance by 26.3% and 36.1%, respectively, that is significantly higher than those in the corresponding intermediates. These structural features reveal that the former transition structures take on more reactant-like character than product-like character and the Hammond postulate[23] predicts that the former should have a lower activation barrier. Second, the C^3–O^1 bond is affected by the conjugated effect of both the carbonyl moiety and the phenyl of **TSd2**, which makes the cleavage of the C^3–O^1 bond for **TSd2** more feasible than for **TSa2**. However, the activation free energy of rate-determining step (**TSd4**) for pathway **a** is 23.4 kcal mol^{-1}, which indicates that the substitution had little effect on this step. Inspection of Fig. 6 shows that a lower barrier was also found for **TSe2** (17.5 and 9.2 kcal mol^{-1}, respectively for the methyl-substituted propargylic acetates and the phenyl-substituted propargylic acetates) to go from the intermediates to the transition states than for **TSb2**. The lower barriers found for **TSe2** may be also due to the Hammond postulate[23] and the conjugated effect of both the carbonyl moiety and the phenyl of **TSe2**. Furthermore, the activation free energy

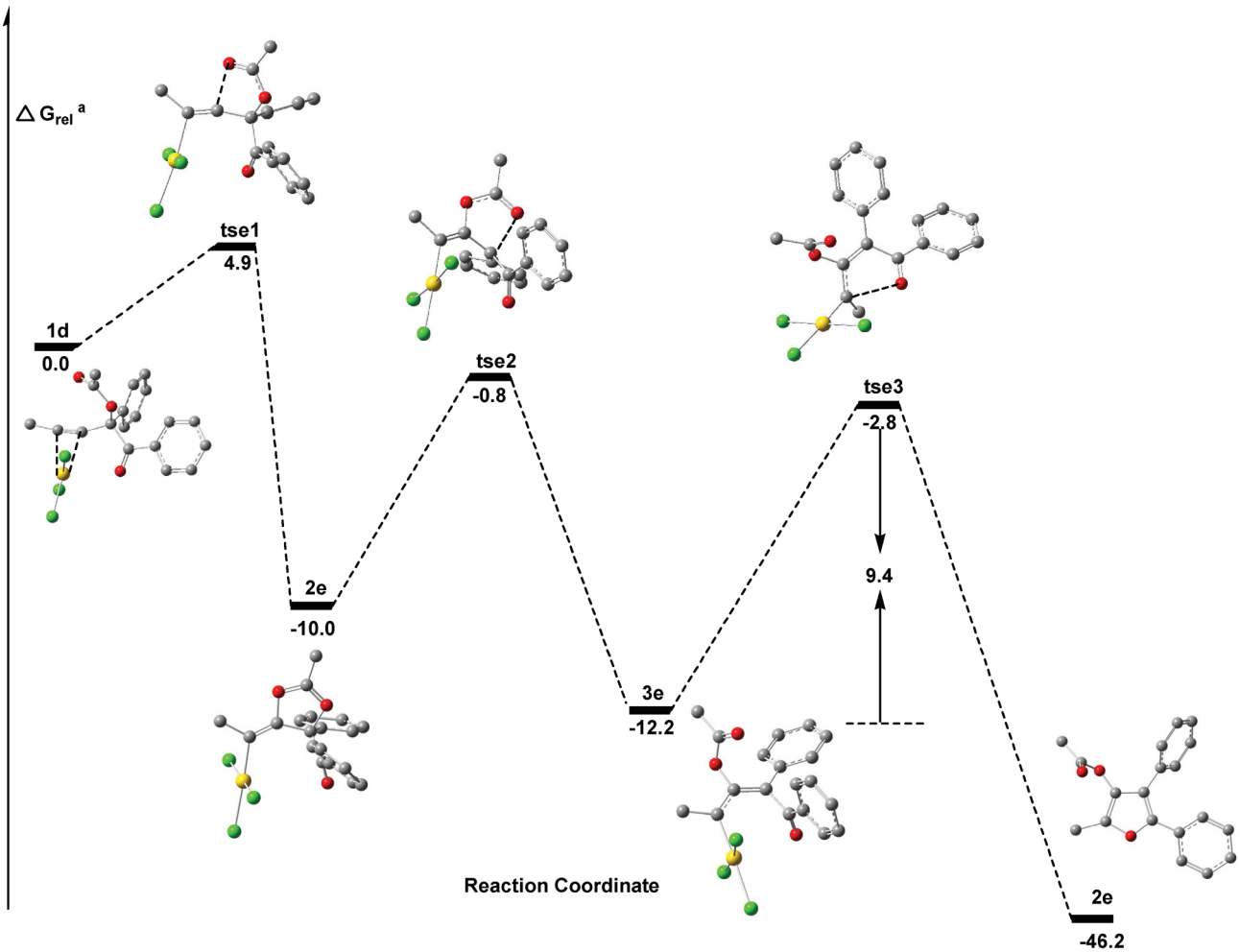

[a] These values, in kcal/mol, were calculated at the BHandHLYP /PCM/6-311++G (d, p)// BHandHLYP /6-31G (d, p) (SDD for Au) level of theory using single-point PCM calculations to model the effect of the solvent (toluene)

Fig. 6 Energy profiles for path **b** of the phenyl-substituted propargylic acetates; the relative energies are given in kcal mol^{-1} (hydrogen atoms are omitted for clarity).

for next step (**TSe3**) was 9.4 kcal mol^{-1}, which indicates that this step should be rate-determining for the phenyl-substituted propargylic acetates, that is different from the reaction of the methyl-substituted propargylic acetates. Moreover, **TSe3** is lower in energy than **TSd4** by 14.0 kcal mol^{-1}, suggesting that the first step of the cycle for the phenyl-substituted propargylic acetates will also be caused by an initial Rautenstrauch-type [1,2]-migration *via* a five-membered ring transition state to form the Au(III) vinyl carbenoid. Subsequent cycloisomerization of this intermediate then provided the corresponding furan **2e**.

Computational Methods

The geometries of all the structures were fully optimized by hybrid density functional theory (DFT) using the GAUSSIAN 03 program suite.[24] Exchange and correlation were treated by the BHandHLYP method, which is based on Becke's half-and-half method[25] and the gradient-corrected correlation functional of Lee and coworkers.[26] This hybrid DFT method has been successfully applied in the mechanistic studies of transition metal- or non-transition metal-catalyzed reactions.[17i,27] The 6-31G [28] basis set with polarization (d) and (p) were selected for all the atoms except gold, for which the Stuttgart–Dresden effective core potential [29] was utilized to accurately account for relativistic effects and to substantially reduce the number of electrons in the system. This basis set has been popularly used in the mechanistic studies of Au-catalyzed reactions and is shown to be quite reliable for optimizing both the geometries and energies.[17g,30] Vibrational frequency calculations at the BHandHLYP/6-31G(d,p) level of theory were used to characterize all of the stationary points as either minima (the number of imaginary frequencies (NIMAG = 0) or transition states (NIMAG = 1)). The relative energies are thus corrected for the vibrational zero-point energies (*ZPE*, not scaled). In several significant cases, intrinsic reaction coordinate (IRC) [31] calculations were performed to unambiguously connect the transition states with the reactants and the products. To include the effect of the solvent on the reactions of interest, the polarized continuum model (PCM) was applied [32–34] and

single-point energy calculations were done at the BHandHLYP/PCM/6-311++G(d,p)//BHandHLYP/6-31G(d,p) (SDD for Au) level of theory using the geometries along the minimum energy pathway. The dielectric constant was assumed to be 2.379 for the bulk solvent toluene.

Conclusions

In summary, this work has provided a theoretical study for the reaction of gold(III)-catalyzed synthesis of highly substituted furans *via* [3,3]-sigmatropic rearrangements and/or [1,2]-acyloxy migration based on propargyl ketones. According to our calculations, whether for the methyl substituted propargylic acetates or the phenyl substituted propargylic acetates, the major pathway of the cycle should involve an initial Rautenstrauch-type [1,2]-migration *via* oxirenium to form an Au(III) vinyl carbenoid. Subsequent cycloisomerization of this intermediate then provides the corresponding furan **2**. Moreover, for the methyl-substituted propargylic acetates, the formation of Au(III) vinyl carbenoid structures is the rate-determining step. However, intramolecular nucleophilic attack and subsequent cycloisomerization to give the final product israte-determining for the phenyl-substituted propargylic acetates. The computational results are in good agreement with the experimental observations of Gevorgyan *et al.*[18] for gold(III)-catalyzed synthesis of highly substituted furans based on propargyl ketones.

Acknowledgements

This research has been supported by the Fundamental Research Funds for the Central Universities (Grant No. Izujbky-2009-29, Grant No. Izujbky-2010-37) to R. Fang and L. Z. Yang and the National Natural Science Foundation of China (Grant No. 20873102) to Y. C. Wang. The high performance computing facility at the Gansu Computing Center is also acknowledged.

Notes and references

1 (*a*) X. L. Hou, H. Y. Cheung, T. Y. Hon, P. L. Kwan, T. H. Lo, S. Y. T. Tong and H. N. C. Wong, *Tetrahedron*, 1998, **54**, 1955; (*b*) X. L. Hou, Z. Yang, H. N. C. Wong, In *Progress in Heterocyclic Chemistry*, Vol. 14 (ed.: G. W. Gribble, T. L. Gilchrist), Pergamon, Oxford, 2002, 139; (*c*) S. F. Kirsch, *Org. Biomol. Chem.*, 2006, **4**, 2076; (*d*) R. C. D. Brown, *Angew. Chem., Int. Ed.*, 2005, **44**, 850.

2 (*a*) L. A. Paquette and P. C. Astles, *J. Org. Chem.*, 1993, **58**, 165; (*b*) P. A. Jacobi, K. M. Touchette and H. G. Selnick, *J. Org. Chem.*, 1992, **57**, 6305; (*c*) L. A. Paquette, A. M. Doherty and C. M. Rayner, *J. Am. Chem. Soc.*, 1992, **114**, 3910; (*d*) S. F. Martin and P. W. Zinke, *J. Org. Chem.*, 1991, **56**, 6600; (*e*) S. P. Tanis, E. D. Robinson, M. C. McMills and W. Watt, *J. Am. Chem. Soc.*, 1992, **114**, 8349.

3 B. Gabriele, G. Salerno and E. Lauria, *J. Org. Chem.*, 1999, **64**, 7687 and references therein.

4 D. Végh, P. Zalupsky and J. Kováč, *Synth. Commun.*, 1990, **20**, 1113.

5 (*a*) B. Seiller, C. Bruneau and P. H. Dixneuf, *J. Chem. Soc., Chem. Commun.*, 1994, 493; (*b*) H. Kücükbay, B. Cetinkaya, S. Guesmi and P. H. Dixneuf, *Organometallics*, 1996, **15**, 2434; (*c*) B. Seiller, C. Bruneau and P. H. Dixneuf, *Tetrahedron*, 1995, **51**, 13089.

6 Y. H. Liu, F. J. Song, Z. Q. Song, M. N. Liu and B. Yan, *Org. Lett.*, 2005, **7**, 5408.

7 (*a*) A. S. K. Hashmi, *Angew. Chem., Int. Ed.*, 1995, **34**, 1581; (*b*) A. S. K. Hashmi, T. L. Ruppert, T. Knofel and J. W. Bats, *J. Org. Chem.*, 1997, **62**, 7295; (*c*) A. S. K. Hashmi, L. Schwarz, J. H. Choi and T. M. Frost, *Angew. Chem., Int. Ed.*, 2000, **39**, 2285; (*d*) S. Ma and L. Li, *Org. Lett.*, 2002, **4**, 941; (*e*) S. Ma and Z. Yu, *Angew. Chem., Int. Ed.*, 2002, **41**, 1775; (*f*) S. Ma, J. Zhang and L. Lu, *Chem. Eur. J.*, 2003, **9**, 2447; (*g*) M. H. Suhre, M. Reif and S. F. Kirsch, *Org. Lett.*, 2005, **7**, 3925.

8 (*a*) Y. Fukuda, H. Shiragami, K. Utimoto and H. Nozaki, *J. Org. Chem.*, 1991, **56**, 5816; (*b*) A. V. Kelin and V. Gevorgyan, *J. Org. Chem.*, 2002, **67**, 95; (*c*) A. W. Sromek, A. V. Kelin and V. Gevorgyan, *Angew. Chem. Int. Ed.*, 2004, **43**, 2280.

9 T. L. Yao, X. X. Zhang and R. C. Larock, *J. Am. Chem. Soc.*, 2004, **126**, 11164.

10 (*a*) N. Marion and S. P. Nolan, *Angew. Chem., Int. Ed.*, 2007, **46**, 2750–2752; (*b*) J. Marco-Contelles and E. Soriano, *Chem. Eur. J.*, 2007, **13**, 1350–1357.

11 (*a*) A. Correa, N. Marion, L. Fensterbank, M. Malacria, S. P. Nolan and L. Cavallo, *Angew. Chem., Int. Ed.*, 2008, **47**, 718–721; (*b*) N. Marion and *et al.*, *Chem. Eur. J.*, 2009, **15**, 3243–3260.

12 (*a*) V. Mamame, T. Gress, H. Krause and A. Fürstner A., *J. Am. Chem. Soc.*, 2004, **126**, 8654–8655; (*b*) J M. J. Johansson, D. J. Gorin, S. T. Staben and F. D. Toste, *J. Am. Chem. Soc.*, 2005, **127**, 18002–18003; (*c*) D. J. Gorin, P. Dubé and F. D. Toste, *J. Am. Chem. Soc.*, 2006, **128**, 14480–14481; (*d*) N. Marion, P. de Frémont, G. Lemière, E. D. Stevens, L. Fensterbank, M. Malacria and S. P. Nolan, *Chem. Commun.*, 2006, 2048–2050; (*e*) A. Buzas and F. Gagosz, *Org. Lett.*, 2006, **8**, 515–518; (*f*) C. A. Witham, P. Mauleón, N. D. Shapiro, B. D. Sherry and F. D. Toste, *J. Am. Chem. Soc.*, 2007, **129**, 5838–5839; (*g*) C. H. M. Amijs, V. López-Carrillo and A. M. Echavarren, *Org. Lett.*, 2007, **9**, 4021–4024.

13 (*a*) C. Fehr and J. Galindo, *Angew. Chem., Int. Ed.*, 2006, **45**, 2901–2904; (*b*) A. Fürstner and P. Hannen, *Chem. Eur. J.*, 2006, **12**, 3006–3019; (*c*) C. Fehr, B. Winter and I. Magpantay, *Chem. Eur. J.*, 2009, **15**, 9773–9784.

14 (*a*) L. Zhang, *J. Am. Chem. Soc.*, 2005, **127**, 16804–16805; (*b*) N. Marion, S. Díez-González, P. de Frémont, A. R. Noble and S. P. Nolan, *Angew. Chem., Int. Ed.*, 2006, **45**, 3647–3650; (*c*) A. Buzas and F. Gagosz, *J. Am. Chem. Soc.*, 2006, **128**, 12614–12615; (*d*) L. Zhang and S. Wang, *J. Am. Chem. Soc.*, 2006, **128**, 1442–1443.

15 (*a*) X. Huang, T. de Haro and C. Nevado, *Chem. Eur. J.*, 2009, **15**, 5904–5908; (*b*) G. Li and L. Zhang, *J. Am. Chem. Soc.*, 2008, **130**, 3740–3741; (*c*) K.-G. Ji, X.-Z. Shu, J. Chen, S.-C. Zhao, Z.-J. Zheng, L. Lu, X.-Y. Liu and Y.-M. Liang, *Org. Lett.*, 2008, **10**, 3919–3922.

16 (*a*) E. J. Cho and D. Lee, *Adv. Synth. Catal.*, 2008, **350**, 2719–2723; (*b*) K. Ohe, M. Fujita, H. Matsumoto, Y. Tai and K. Miki, *J. Am. Chem. Soc.*, 2006, **128**, 9270–9271.

17 (*a*) D. J. Gorin and F. D. Toste, *Nature*, 2007, **446**, 395; (*b*) A. Stephen and K. Hashmi, *Angew. Chem., Int. Ed.*, 2008, **47**, 6754; (*c*) O. N. Faza, C. S. López, R. Álvarez and R. de Lera, *J. Am. Chem. Soc.*, 2006, **128**, 2434; (*d*) C. Nieto-Oberhuber, M. P. Munoz, E. Bunuel, C. Nevado, D. J. Cárdenas and A. M. Echavarren, *Angew. Chem., Int. Ed.*, 2004, **43**, 2402; (*e*) Y Xia, A. S. Dudnik, V. Gevorgyan and Y. Li, *J. Am. Chem. Soc.*, 2008, **130**, 6940–6941; (*f*) G. Lemière, V. Gandon, N. Agenet, J. P. Goddard, A. de Kozak, C. Aubert, L. Fensterbank and M. Malacria, *Angew. Chem., Int. Ed.*, 2006, **45**, 7596–7599; (*g*) F. Shi, X. Li, Y. Xia, L. Zhang and Z. Yu, *J. Am. Chem. Soc.*, 2007, **129**, 15503–15512; (*h*) P. H. Cheong, P. Morganelli, M. R. Luzung, K. N. Houk and F. D. Toste, *J. Am. Chem. Soc.*, 2008, **130**, 4517–4526; (*i*) R. Fang, C.-Y. Su, C. Zhao and D. L. Phillips, *Organometallics*, 2009, **28**, 741–748; (*j*) M. Lein, M. Rudolph, A. S. K. Hashmi and P. Schwerdtfeger, *Organometallics*, 2010, **29**, 2206–2210; (*k*) M. Pernpointner and A. S. K. Hashmi, *J. Chem. Theory Comput.*, 2009, **5**, 2717–2725.

18 T. Schwier, A. W. Sromek, D. M. L. Yap, D. Chernyak and V. Gevorgyan, *J. Am. Chem. Soc.*, 2007, **129**, 9868–9878.

19 (*a*) A. S. K. Hashmi and G. Hutchings, *Angew. Chem., Int. Ed.*, 2006, **45**, 7896; (*b*) C. Nieto-Oberhuber, S. López, M. P. Muñoz, D. J. Cárdenas, E. Buñuel, C. Nevado and A. M. Echavarren, *Angew. Chem., Int. Ed.*, 2005, **44**, 6146; (*c*) F.-Q. Shi, X. Li, Y. Xia, L. Zhang and Z. Yu, *J. Am. Chem. Soc.*, 2007, **129**, 15503; (*d*) P. Mauleón, J. L. Krinsky and F. D. Toste, *J. Am. Chem. Soc.*, 2009, **131**, 4513.

20 L. Zhang, *J. Am. Chem. Soc.*, 2005, **127**, 16804.

21 I. Nakamura, T. Sato and Y. Yamamoto, *Angew. Chem., Int. Ed.*, 2006, **45**, 4473.

22 P. Dube and F. D. Toste, *J. Am. Chem. Soc.*, 2006, **128**, 12062.

23 G. S. Hammond, *J. Am. Chem. Soc.*, 1955, **77**, 334.

24 M. J. Frisch,, *et al.*, *GAUSSIAN 03 (Revision E01)*, Gaussian, Inc., Pittsburgh PA, 2004.

25 A. D. Becke, *J. Chem. Phys.*, 1993, **98**, 1372.

26 C. Lee, W. Yang and R. G. Parr, *Phys. Rev. B*, 1988, **37**, 785.

27 (*a*) T. N. Truong and W. Duncan, *J. Chem. Phys.*, 1994, **101**, 7403; (*b*) Q. Zhang, R. Bell and T. N. Truong, *J. Phys. Chem.*, 1995, **99**, 592;

(*c*) J. L. Durant, *Chem. Phys. Lett.*, 1996, **256**, 595; (*d*) B. J. Lynch, P. L. Fast, M. Harris and D. G. Truhlar, *J. Phys. Chem. A*, 2000, **104**, 4811; (*e*) J. Espinosa-García, *J. Am. Chem. Soc.*, 2004, **126**, 920; (*f*) U. Wille, C.-S. Tan and E.-K. Mucke, *J. Org. Chem.*, 2008, **73**, 5821; (*g*) R. Fang, Z. Ke, Y. Shen, C. Zhao and D. L. Phillips, *J. Org. Chem.*, 2007, **72**, 5139.
28 (*a*) V. A. Rassolov, M. A. Ratner, J. A. Pople, P. C. Redfern and L. A. Curtiss, *J. Comput. Chem.*, 2001, **22**, 976; (*b*) V. A. Rassolov, J. A. Pople, M. A. Ratner and T. L. Windus, *J. Chem. Phys.*, 1998, **109**, 1223.
29 (*a*) D. Andrae, U. Häussermann, M. Dolg, H. Stoll and H. Preuss, *Theor. Chim. Acta*, 1990, **77**, 123; (*b*) the detail basis set for Au were given in the Supporting information.
30 (*a*) K. Ando, *J. Org. Chem.*, 2010, **75**, 8516–8521; (*b*) G. Kovács, A. Lledós and G. Ujaque, *Organometallics*, 2010, **29**, 3252–3260.
31 C. Gonzalez and H. B. Schlegel, *J. Chem. Phys.*, 1989, **90**, 2154.
32 J. Tomasi and M. Persico, *Chem. Rev.*, 1994, **94**, 2027.
33 T. Mineva, N. Russo and E. Sicilia, *J. Comput. Chem.*, 1998, **19**, 290.
34 M. Cossi, G. Scalmani, N. Rega and V. Barone, *J. Chem. Phys.*, 2002, **117**, 43.

